

Master Copy

A LARGE ACCEPTANCE MAGNETIC SPECTROMETER FOR CEBAF

CEBAF-PR-87-015 VWC3
Bernhard Mecking
A large acceptance \ for CEBAF
* 020592000096192

Bernhard A. Mecking

CEBAF
12070 Jefferson Avenue
Newport News, Virginia 23606



Abstract

A large acceptance magnetic spectrometer for the investigation of electron- and photon-induced nuclear reactions at CEBAF is described.

I. Introduction

The scientific program for the CEBAF 4 GeV electron accelerator aims at studying the structure and the motion of the nuclear constituents. The experimental equipment that has been proposed consists of focusing magnetic spectrometers with relatively small acceptances ($\Delta\Omega \approx 10^{-2} \cdot 4\pi$, $\Delta p/p \approx 10\%$) but high momentum resolution ($\Delta p/p \leq 10^{-4}$) and a large acceptance spectrometer. In the following report, the physics motivation for a large acceptance detector, the general design criteria and technical details of the detector will be discussed.

II. Physics Motivation

Electron scattering experiments have provided most of what we know about the structure of nuclei. However, our knowledge is limited to the electromagnetic structure of ground states and excited states of nuclei (explored in (e,e') experiments) and to some aspects of the nuclear single-particle structure (explored in (e,e'p) experiments). Very little is known about the many-body aspects of the nucleus, like e.g. the structure of bound nucleons, the origin of short-range correlations or the propagation of meson or nucleon resonances in the nuclear medium. The reason for this limitation is largely due to the technical features of the available experimental facilities:

- a) The low duty-cycle of existing electron accelerators limits coincidence experiments to a narrow kinematical region where a sufficient signal-to-noise ratio can be achieved. It also makes the operation of large acceptance detectors inefficient because their counting rates are limited by the instantaneous background rates.
- b) High accuracy in charged particle detection can only be achieved in small acceptance magnetic spectrometers.

Important technical developments have changed this picture

- a) Electron accelerators with 100% duty-cycle are being built.
- b) The quality and versatility of large acceptance detectors has improved dramatically.

A large acceptance detector will be required for the detection of multiple particle final states and for measurements at limited luminosity. Examples will be given for these experiments:

1. Multiple Particle Final States

For reactions involving several particles in the final state, high detection efficiency and a model-

free analysis of the data can only be achieved by using a detector with a wide coverage of the angular and energy range for all outgoing particles. Examples for reactions which are of special interest for CEBAF are:

- a) Hadronic final states in inclusive electron scattering off nuclei. Single arm electron scattering and (e,e'p) coincidence experiments have generated puzzles which can only be solved by a detailed investigation of the hadronic final state. Using a large acceptance detector, a bias-free investigation can be carried out by triggering on the scattered electron only. In the off-line analysis, the inclusive scattering cross section can then be decomposed into its hadronic channels. With increasing energy loss for the electron, the following phenomena can be studied:
 - (1) Electron scattering at large negative y (y = momentum component of the struck nucleon parallel to the direction of the virtual photon q) yields higher cross sections than expected from standard nuclear models. The excess cross section can be explained by high momentum components in the nuclear wave function (+ emission of a single nucleon) or by interaction of the virtual photon with quark clusters (+ emission of nucleon pairs or nucleon clusters like deuterons etc.). These two possibilities can be distinguished by detecting the hadronic final state.
 - (2) Quasi-free electron scattering off bound nucleons (requiring the hadronic final state to contain a recoiling nucleon around the direction of q). A long-standing problem is the failure of the Coulomb sum rule to account correctly for the number of protons in the nucleus. This has been interpreted as a change of the nucleon form factor in the nuclear medium or as evidence for a direct interaction of the virtual photon with a six-quark bag.
 - (3) Multi-nucleon emission (requiring the hadronic final state to contain ≥ 2 nucleons). Two nucleon emission is assumed to be responsible for filling the dip between the quasi-free peak and the Δ -peak; there should also be strength in the Δ -region due to Δ -excitation with subsequent Δ -N interaction.
 - (4) Production and propagation of non-strange (Λ and higher nucleon resonances) and strange (Λ , Σ and their excited states) 3-quark objects in nuclei (requiring the hadronic final state to be a πN , ηN , $\pi\pi N$, $K\Lambda$ etc. system in the appropriate mass range). Modifications of the properties of these resonances in the nuclear medium can be studied.
 - (5) Deep inelastic electron scattering. The aim of this program is to study the hadronization of the struck quark in the region of large momentum and energy transfer and to understand how the inclusive cross section is built up out of individual hadronic channels.

Good particle identification for multiple particle final states down to very small angles ($\theta \leq 5^\circ$) is important for this program.

- b) Photo- and electro-excitation of the higher nucleon resonances. The harmonic oscillator quark model with QCD motivated additions (like a one-gluon exchange term) predicts, in addition to the known nucleon resonances, many states which have not been observed. A plausible explanation²⁾ is that these states decouple from the πN elastic channel and can, therefore, not be observed in elastic πN scattering. Since, on the other hand, the photocoupling is still strong, photoexcitation becomes the only available formation mechanism. Promising decay channels are:



- c) Photo- (and electro-) excitation of vector mesons: $\gamma N + V N$ ($V = \rho, \omega, \phi$). An important goal of this program is to measure the γ -V coupling constant to get information on the hadronic content of the photon³⁾ and its variation with Q^2 . In addition, the vector meson coupling to the nucleon can be determined. In boson exchange models of the nucleon-nucleon interaction, this quantity is of fundamental importance for the short range part of the NN-interaction.

- d) Hyperon production and interaction: $\gamma N + K \Lambda$ (Σ)
The basic cross sections and coupling constants for these reactions have to be known for the analysis of the electromagnetic excitation of hypernuclei. Using the outgoing kaon to determine the Λ kinematics, a tagged low intensity hyperon beam can be generated. The production rates are large enough so that the decay and the interaction of the produced hyperon can be studied in the reactions:

- (1) $\Lambda p + \Lambda p$ (elastic scattering)
Because of its short decay length, the interaction of low momentum Λ 's is best studied in the production target. Using the $\gamma p + K^+ \Lambda$ reaction for Λ production, about 500 Λ scattering events can be observed per day in a large acceptance spectrometer.
- (2) $\gamma d + K^+ \Lambda n$
This reaction allows also to study the ΛN interaction. Especially interesting is the search for long-lived $S=-1$ dibaryons; the masses of these objects⁴⁾ have been predicted to be around the Σ -cusp⁴⁾.
- (3) Radiative hyperon decay: $\Lambda^*(1520) + \gamma \Lambda$ and $\Lambda^*(1520) + \gamma \Sigma$.
Using a tagged photon beam, about $5 \cdot 10^5$ $\Lambda^*(1520)$ can be produced per day. The radiative decay width yields a sensitive test of the quark structure of the system.

- e) Exclusive photoreactions on few-body systems



The basic properties of bound 3-quark systems are best studied in few-body nuclei because the nuclear structure can be calculated exactly (at least in the framework of a non-relativistic potential model). Interesting questions are the off-shell behavior of the γNN^* vertex, the structure of the $N^* N$ interaction, the existence of dibaryons⁵⁾ and of 3-body forces⁶⁾ in ${}^3\text{He}$.

- f) Interaction parameters of unstable particles.
The measurement of the Λ -dependence of total production cross sections for unstable particles will determine their total hadronic cross sections. In contrast to hadronic production reactions, the electromagnetic production offers the big advantage that the interaction of the incident projectile is so weak that the Λ -dependence of the cross section can be interpreted directly in terms of the interaction of the produced particle. Especially interesting is a comparison of the hadronic interaction of the $\eta(549)$ and $\eta'(958)$ which are supposed to be different mixtures of the same $SU(3)$ states. The large η' mass is attributed to a sizeable exotic (gluonic or hybrid) component; this should show up as a difference in the hadronic behavior of η and η' .

A comprehensive study of the reactions b) - e) requires the use of polarized beams (longitudinally polarized electrons, linearly and circularly polarized photons) and polarized targets (polarized protons, vector- and tensor-polarized deuterons).

2. Limited Luminosity

The luminosity (target density \cdot beam intensity) limitation can be due to the target or due to the beam.

- a) Limitation due to the beam intensity.
Experimental programs using secondary particle beams (real γ, μ, π, K) need large acceptance coverage to collect sufficient count rate, independent of the number of particles in the final state. Especially important are tagged photon beam experiments where the intensity has to be limited to $\approx 10^7$ tagged γ /sec to keep accidental coincidences small.
- b) Limitation due to the use of a polarized target.

- (1) Polarized solid state hydrogen and deuterium targets.
For present solid state polarized targets (ammonia or deuterated ammonia) the luminosity has to be kept low ($\approx 10^{28} \text{ cm}^{-2} \text{ sec}^{-1}$ for tensor-polarized deuterium, $\approx 10^{25} \text{ cm}^{-2} \text{ sec}^{-1}$ for polarized hydrogen) in order to avoid a reduction of the polarization due to beam heating and radiation damage.
- (2) Polarized gas targets.
The disadvantages of polarized solid targets (high magnetic fields, nuclear background, low temperatures, limited to hydrogen and deuterium) can, in principle, be avoided by using a low density polarized gas target in combination with a high intensity electron beam. A dedicated electron storage ring would clearly be ideal for this program. However, the rapid progress in gas target technology will make experiments in the CEBAF external electron beam possible.

Compared to a storage ring, polarized gas target experiments in an external beam will have lower luminosity. However, there are also some important advantages:

- a) No difficulties to achieve longitudinal electron polarization.
- b) Modest vacuum requirements \rightarrow less differential pumping will be required.
- c) Greater flexibility in the arrangement of the experimental apparatus.
- d) Since the beam passes through the target only once, small beam losses are acceptable \rightarrow thin

windows or very small diameter openings for bottle targets can be used.

These features should also make it possible to achieve higher target density than in a storage ring. A minimum density of $\approx 10^{16}$ atoms/cm³ is necessary to give reasonable counting rate. At this luminosity ($\approx 10^{30}$ cm⁻² sec⁻¹), the combination of a polarized gas target and a large acceptance spectrometer will be useful for the investigation of reactions induced by quasi-real photons.

For ³He, the densities already reached^{8),9)} give a luminosity of several 10^{30} cm⁻² sec⁻¹. This luminosity is high enough to allow for an extensive nuclear physics program especially with a large acceptance detector. Polarized ³He targets can be used to investigate the structure of the 3-body system or as a source of polarized neutrons. The following experiments are of special interest:

- (a) ³He($\vec{e}, e'n$)pp to determine the electric form factor of the neutron G_E^n .
- (b) ³He($\vec{e}, e'\Delta^0$)pp to determine the C2/M1 ratio for the $n\Delta^0$ transition.

III. General Design Considerations

A large acceptance detector that is suitable for a broad range of photonuclear experiments using electron and photon beams should have the following properties:

1. Homogeneous coverage of a large angular and energy range for charged particles (magnetic analysis), photons (total absorption counters) and possibly neutrons.
2. Good momentum and angular resolution (+ magnetic analysis for charged particles).
3. Good particle identification properties in the momentum range of interest (+ combination of magnetic analysis and time-of-flight).
4. No transverse magnetic field at the beam axis (to avoid sweeping e^+e^- -pairs into the detector).
5. No magnetic field in the target region to provide for the installation of polarized (solid state or gaseous) targets requiring their own guiding field or other complicated equipment (cryogenic or track sensitive targets, vertex detectors etc.).
6. Symmetry around the beam axis to facilitate triggering and event reconstruction.
7. Large $\int B \cdot dl$ for forward going particles to account for the Lorentz-boost.
8. High luminosity and count rate capability. The detector should operate in the difficult background environment encountered in electron scattering experiments. The background caused by a tagged bremsstrahlung photon beam ($N_\gamma \approx 10^7$ /sec) is much lower and will give no additional constraints.
9. Open geometry for the installation of a long time-of-flight path for neutron detection.

The consequences of these requirements for the choice of the magnetic field configuration have been studied. Transverse dipole, longitudinal solenoidal and toroidal fields have been considered. In all cases, the target has been assumed to be inside the magnetic field volume. The results are summarized in table I. To fulfill requirements #2 and #3, a large $\int B \cdot dl$ and a long time-of-flight (ToF) path is

necessary. This can be achieved by all field configurations. The transverse dipole field is ruled out by #4 in combination with #8; it also violates #6. The solenoid which has become the standard magnetic field configuration at e^+e^- colliders violates requirements #5, #7 and #9; therefore, it has to be ruled out. The only configuration that fulfills all requirements is the toroidal magnetic field. Since the ϕ -range for magnetic analysis is limited due to the coils, the detection efficiency for high multiplicity (> 4) final states will be low. However, in view of the present CEBAF program, it seems to be more important that the detector will be capable to complement the standard spectrometer set-up instead of trying to specialize it for high multiplicity reactions.

IV. The Large Acceptance Detector

The solution that has been proposed for the CEBAF Large Acceptance Spectrometer (LAS) is a superconducting toroidal magnet equipped with drift chambers, scintillation counters and shower counters. A description of the main features of the LAS will be given below.

1. Toroidal Magnet

The toroidal magnet consists of 8 coils arranged around the beam line to produce essentially a magnetic field in ϕ -direction. The size, field strength and coil shape were determined on the basis of the physics requirements (see table II for details). A perspective view of the magnet is shown in fig. 1, the coil shape is given in fig. 2. Each superconducting coil is embedded in a rigid coil case (about 4 meter long and 2 meter wide). Details of the coil layout, construction and protection have been worked out during the Workshop on CEBAF Spectrometer Magnet Design and Technology¹⁰⁾. The coils are housed in individual cryostats to facilitate manufacturing, assembly and testing. For the magnetic field calculations, the finite size of the coil was simulated by adding up the contributions of 4 discrete conductor loops (as indicated in fig. 2). The r -dependence of the magnetic field is given in fig. 3 for different z -positions. In a cylinder of 50 cm diameter around the axis the magnetic field is ≤ 10 Gauss. As demonstrated in fig. 4, the field lines are essentially circles (corresponding to a pure ϕ -field) with important deviations close to the coils. Figure 5 gives the integral over the ϕ -component of the field as a function of the particle emission angle θ . For forward going particles, the integral is about twice as high as for particles going sideways.

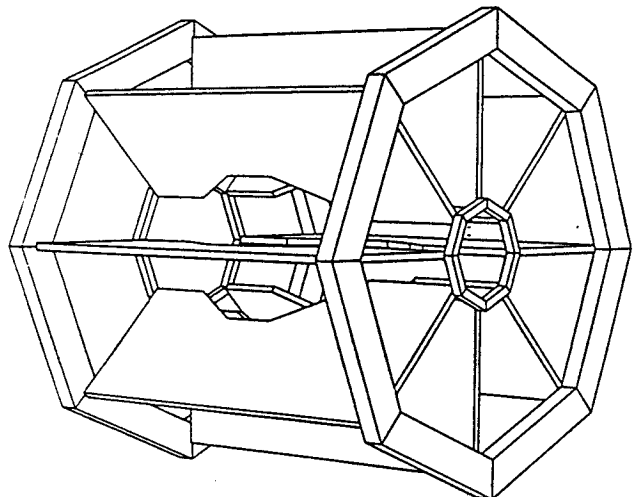


Figure 1 Perspective view of the toroidal magnet.

Coils
loops
Curre
B unit
B step
x(3)

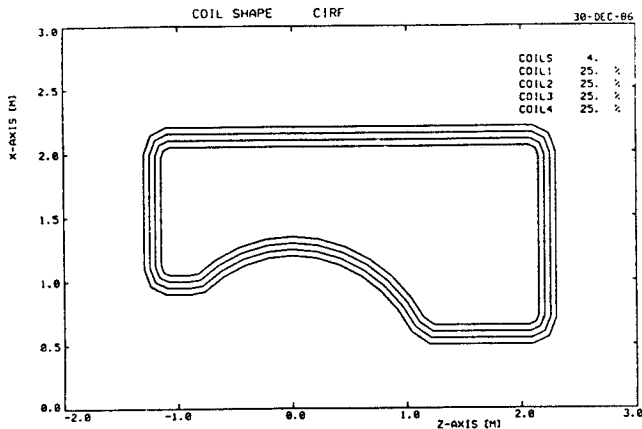


Figure 2 Coil shape. The superconductor is represented by 4 individual current loops.

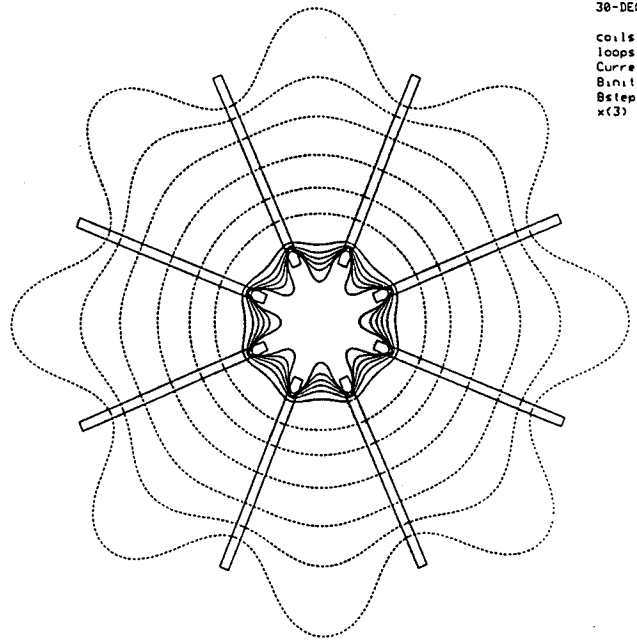


Figure 4 Field lines (giving the direction of the magnetic field) for $z=1.8m$ (forward part of the magnet).

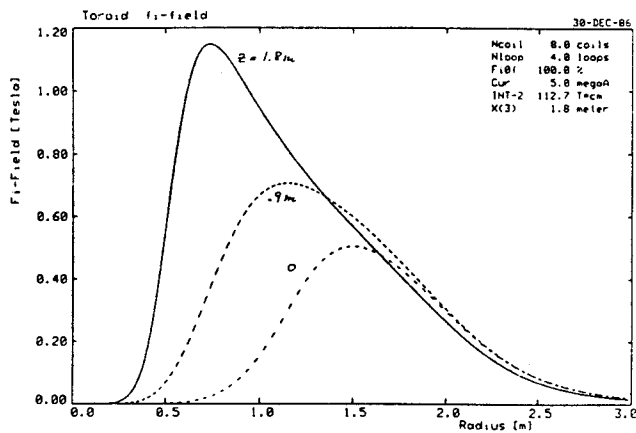


Figure 3 Radial dependence of B_z for $z=0, 0.9 m$ and $1.8 m$ ($z=0$ corresponds to the target position) and $\phi=0$ (corresponding to the mid-plane between two coils).

The inner section of the coil is circular to avoid transverse (in ϕ -direction) motion of those outgoing particles that do not form a 90° angle with the conductor. This is demonstrated in fig. 6a for a rectangular coil shape (the current has been adjusted to make the total bend angle the same as for the circular coil). The transverse deflection depends on the angles θ (relative to the axis), ϕ (azimuthal angle) and on the particle momentum and polarity. The resulting loss of events will be difficult to correct. By using a circularly shaped coil, the angle of incidence can be kept normal to the coil, independent of θ . As shown in fig. 6b, the transverse particle motion is very much reduced.

2. Particle detection system

The proposed particle detection system consists of drift chambers to determine the track of charged particles, scintillation counters for the trigger and for time-of-flight, and shower counters to detect photons. A side view of the detection system is given in fig. 7, a cut in the target region in fig. 8. Note that all 8 segments are individually instrumented to form 8 independent magnetic spectrometers. This will facilitate track reconstruction in a large background environment.

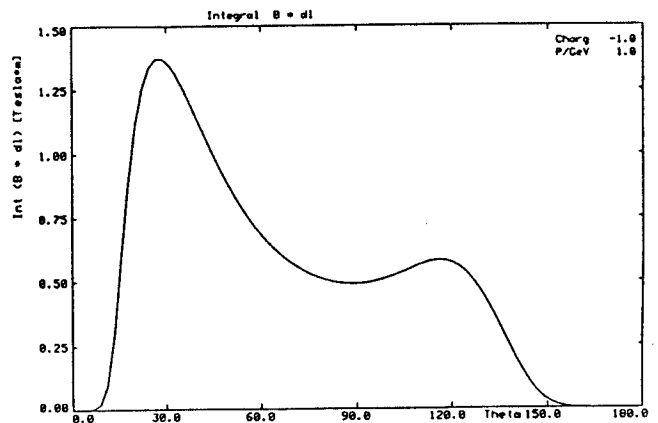


Figure 5 θ -dependence of the integral $\int B \cdot dr$. θ is the particle emission angle relative to the axis; the target has been assumed to be at $z = 0 m$. Particle momentum $1 GeV/c$.

2.1 Tracking chambers

Charged particles are tracked by planar wire chambers. Each planar chamber consists of 4 layers of sense wires stretched in ϕ -direction. The position of the hit along the sense wire will be determined by charge division.

2.2 Scintillation Counters

The outer planar drift chambers are completely surrounded by scintillation counters. The barrel counters consist of 8×8 counters, each about 400 cm long, 20 cm wide, and 5 cm thick. The counters are viewed by 2" phototubes at both ends for improved timing and position resolution. The endcaps are covered by 8×4 pie-shaped counters, each viewed by one photomultiplier. Because of the high rate, the

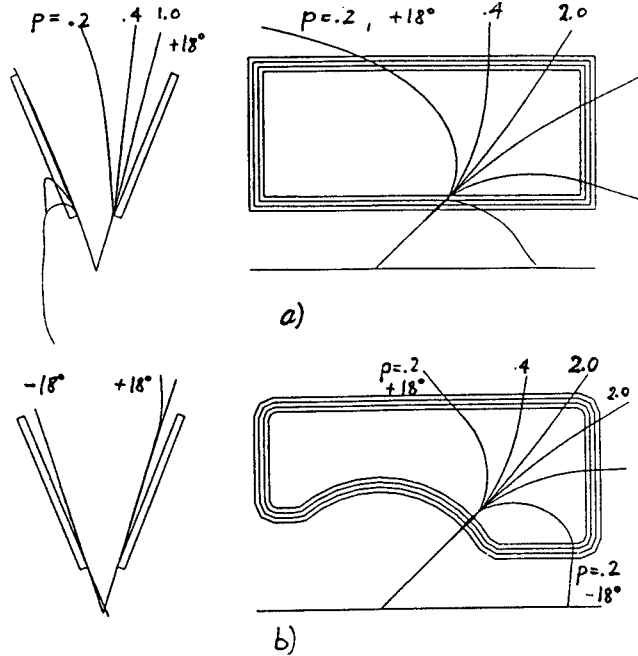


Figure 6 Transverse particle deflection in toroidal magnets for particles with $\theta=40^\circ$, $p=0.2, 0.4$ and 2.0 GeV/c and $\phi=\pm 18^\circ$ ($\phi=0$ corresponds to the mid-plane).
 a) rectangular coil shape. Particles that are deflected away from the axis by the ϕ -component of the field are bent back to the mid-plane; particles that are deflected away towards the axis are bent towards the coils and are lost.
 b) coil with a circular inner section. Note that there is no transverse motion at inner edge of the coil.

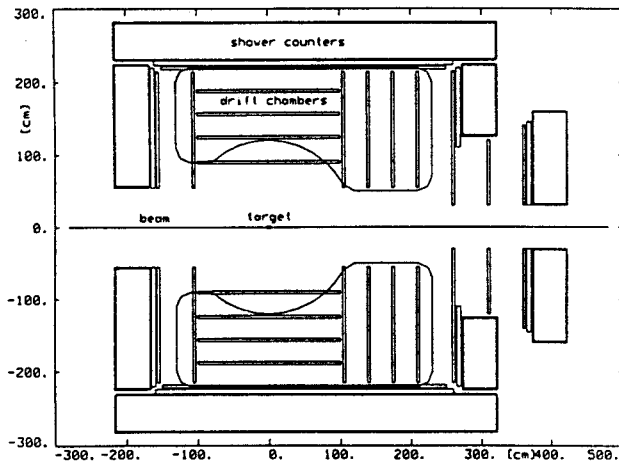


Figure 7 Transverse view of the particle detection system.

forward endcap counters are split into two rings: one ring at large and one at small angles. The scintillation counters serve the double purpose of providing the trigger and the time-of-flight information. Also, a fraction of the high energy neutrons ($\approx 5\%$) will interact in the scintillation counters and will thus be detected.

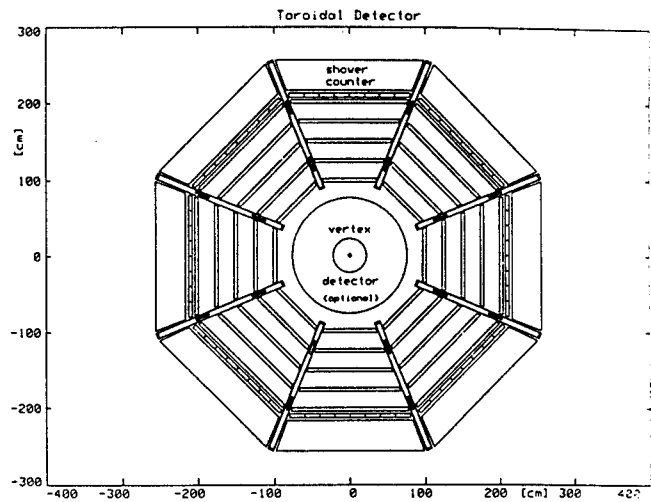


Figure 8 View of the detection system in the direction of the beam for $z=0$ (target position).

2.3 Shower Counter

The detector is surrounded by shower counters for the detection of showering particles like high energy photons from the decay of hadrons like π^0, η, η' etc. Due to the size and the weight of the counter (≈ 80 m², ≈ 100 tons), inexpensive materials and construction techniques have to be used (e.g., a sandwich of lead plates interleaved with active material like scintillators or gas detectors). The expected energy resolution is $\sigma/E_\gamma \lesssim .13/\sqrt{E_\gamma}(\text{GeV})$.

3. Maximum Luminosity

In an electron beam, the main background is caused by electron-electron scattering and wide angle bremsstrahlung. At a luminosity of $10^{28} \text{ cm}^{-2} \cdot \text{sec}^{-1}$, the rate of Møller scattered electrons is estimated to be of the order of $5 \cdot 10^7 \text{ sr}^{-1} \cdot \text{sec}^{-1}$. Since the energies are low, the electrons are bent back even by the small magnetic fringe field. A fraction of the electrons will, however, radiate photons that will subsequently generate spurious signals in the chambers. The total integrated flux of photons due to wide angle bremsstrahlung has been estimated to be of the order of $10^6 \text{ sr}^{-1} \cdot \text{sec}^{-1}$ (luminosity $10^{28} \text{ cm}^{-2} \cdot \text{sec}^{-1}$, $E_0 = 2$ GeV, ^{12}C target, all photons above 10 keV). Compared to these electromagnetic background rates, the hadronic rates are nearly negligible. The total rate of electrons scattered into the angular range $15^\circ \leq \theta \leq 150^\circ$ due to hadronic processes is less than 1000/sec. The total hadron rate (mainly produced by quasi-real photons) is $\approx 5 \cdot 10^4/\text{sec}$. On the basis of these counting rate estimates and also due to past operating experience of a large acceptance detector at an electron accelerator¹¹⁾, one can expect that the detector can be operated at a luminosity of $\approx 10^{28} \text{ cm}^{-2} \cdot \text{sec}^{-1}$ (corresponding to a $1 \mu\text{A}$ electron beam on a 1 mg/cm^2 target).

There will be no difficulties to operate the detector at tagged photon beam intensity ($\approx 10^7 \gamma/\text{sec}$). (At this photon beam intensity, the hadronic production rate is about the same as in electron beam

with a luminosity of $10^{32} \text{ cm}^{-2} \text{ sec}^{-1}$; however, due to the lack of Møller scattered electrons the background rate is much lower.)

4. Track Resolution

The track resolution has been calculated taking the position resolution of the chambers and multiple scattering into account. The momentum resolution $\Delta p/p$ for known vertex position is shown in fig. 9 for 1 GeV/c particles as a function of the particle emission angle θ . The momentum resolution reaches 0.6% in the forward direction; in the central part, it drops to 1.5% due to the decreasing $|B \cdot dl|$. For known vertex position, $\Delta p/p$ is dominated by multiple scattering; therefore, it is nearly constant in the whole momentum range of interest. The initial angle can be determined with an uncertainty $\Delta\theta \leq 1 \text{ mrad}$ for 1 GeV/c particles (2 mrad for 0.2 GeV/c).

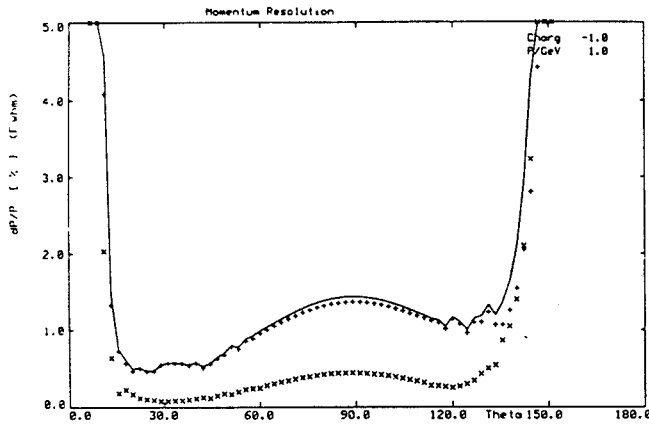


Figure 9 Momentum resolution $\Delta p/p$ (FWHM) as a function of the particle emission angle θ for $p = 1 \text{ GeV/c}$. The vertex is assumed to be known.
 x contribution of the chamber position resolution
 + multiple scattering contribution
 — sum of both contributions.

5. Particle Identification

The combination of momentum and time-of-flight (a time resolution of $\Delta\tau = 200 \text{ psec}$ (sigma) was assumed) gives clean particle identification over a wide momentum range. In the forward direction, pions can be separated from kaons up to 1.5 GeV/c, the limit for kaon/proton separation is 2.5 GeV/c. π/e , π/μ and μ/e separation can be achieved by using the pulse height in the shower counter in addition.

6. Acceptance

Using a Monte Carlo technique, random multiple particle events were generated to determine the acceptance. Examples for single events as they would be reconstructed and displayed on-line by the detector single-event display are presented in figs. 10 and 11. For the calculation of the acceptance, the θ -range of the detector was taken to be $15^\circ \leq \theta \leq 150^\circ$, 20% of the ϕ -range was assumed to be obstructed by the coils. In addition, cuts in the kinetic energy of the emitted particles were applied to account for detection thresholds: $T_{\pi^-} \geq 40 \text{ MeV}$ and $T_{\pi^+} \geq 50 \text{ MeV}$. For the process $\gamma + p \rightarrow F35(1975) + \pi^- + \Delta^{++} + \pi^- + \pi^+ + p$ about 60% of the all $\pi^- \pi^+ p$ events are accepted if only θ

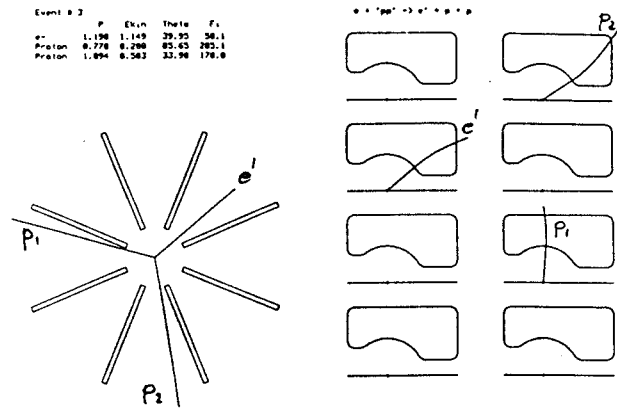


Figure 10 Single event display for a Monte Carlo generated event from the reaction $(e, e'pp)$. $E = 2 \text{ GeV}$, $\theta = 40^\circ$. The left hand side of the display shows a view of the event in the direction of the beam, the r.h.s. presents the tracks in the 8 individual segments.

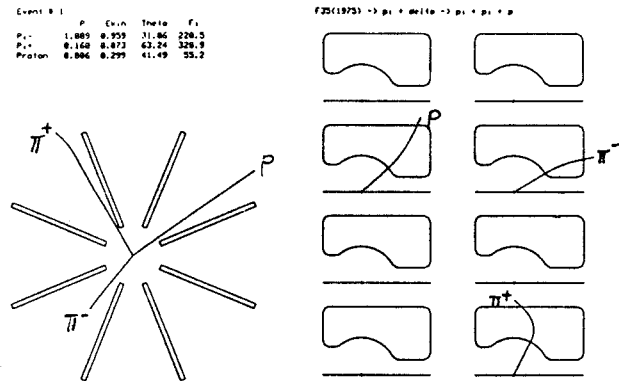


Figure 11 Single event display for a Monte Carlo generated event from the reaction $\gamma p \rightarrow N^* + \pi^- \Delta^{++} + \pi^- \pi^+ p$ induced by real photons. $E_\gamma = 1.6 \text{ GeV}$.

and T_{min} cuts are used. The addition of the ϕ -cuts reduces the total detection efficiency to 30%.

7. Counting Rate Examples

a) $(e, e'X)$
 The counting rate for have been estimated for $^{12}\text{C}(e, e')$ at $E = 2 \text{ GeV}$ and $\theta = 15^\circ$. A luminosity of $10^{32} \text{ cm}^{-2} \text{ sec}^{-1}$ (per nucleon) and 80% ϕ -coverage have been assumed. The total rate of electrons scattered into the angular interval $14^\circ - 16^\circ$ and the energy interval (1.3-2.0) GeV is $\approx 100/\text{sec}$.

b) photon induced reactions
 Combining a tagged photon beam with an intensity of $10^7 \text{ } \gamma/\text{sec}$ and a hydrogen target of 0.5 g/cm^2 ($\approx 7 \text{ cm}$ liquid) results in a total hadronic production rate of $\approx 400 \text{ events/sec}$ ($E_0 = 2 \text{ GeV}$, $\sigma_{\text{tot}} = 140 \text{ } \mu\text{b}$).

8. Layout of End Station B

The detector will be located in end station B. A possible layout of the end station is shown in fig. 12. End station and beam dump are fully shielded to allow for experiments using a high intensity beam on a thin gas target (also to allow for a second high

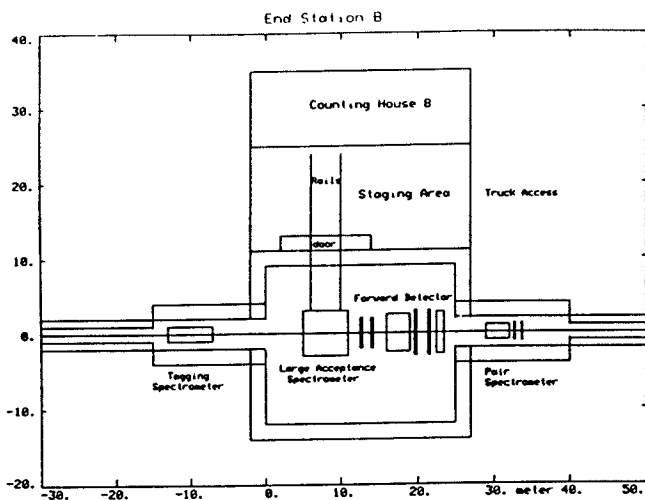


Figure 12 Proposed layout of the low intensity end station B.

intensity experiments in this area). The detector can be moved on rails into an adjacent staging area for extended service. For photon experiments, a vertically deflecting tagging spectrometer is located in an enlarged tunnel section.

V. Summary

A large acceptance magnetic spectrometer has been proposed for the investigation of electron- and photon-induced nuclear reactions at CEBAF. The magnetic field is generated by eight toroidal coils. Charged particles are tracked using scintillation counters and drift chambers; high energy photons are detected by shower counters. The spectrometer will be indispensable for the investigation of multiple particle final states from $(e, e'X)$ reactions and from the decay of excited qq and qqq -states. In addition, it will provide the highest possible counting rate for experiments in which the luminosity is limited due to low target density or low beam intensity.

References

- 1) H.J. Pirner et al., Phys. Rev. Lett. 46 (1981) 1376.
- 2) N. Isgur, Proc. of the 1984 CEBAF Summer Workshop, Newport News, Virginia, ed. by F. Gross and R. R. Whitney, p. 199
- 3) T.H. Bauer et al., Rev. of Mod. Physics, 50 (1978) 261
- 4) M.E. Sainio, AIP Conf. Proc. 150 (1986) 886
- 5) M.P. Locher et al., Adv. in Nucl. Phys., Vol. 17 (1988) 47
- 6) I. Sick, Lecture Notes in Physics 260 (1986) 42
- 7) F. Lenz, Nucl. Phys. B279 (1987) 119

- 8) R.D. McKeown and R.G. Milner, 1985 CEBAF Summer Study, RPAC I, p. 12-45
- 9) R.G. Milner et al., private communication, submitted to Nucl. Instr. and Meth.
- 10) P.G. Marston: Report of the Working Group on the Large Acceptance Spectrometer, Proc. of the Workshop on CEBAF Spectrometer Magnet Design and Technology, Newport News, April 1986, ed. by J. Mougey and P. Brindza
- 11) L.A. Ahrens et al., Nucl. Instr. Meth. 173 (1980) 537.

Table I: Evaluation of magnetic field configurations for a large acceptance spectrometer to be used for electron- and photon-induced reactions

(+ denotes advantage, - drawback)

	Dipole	Solenoid	Toroid
Large solid angle	(+)	++	(+)
No transverse field	--	+	+
No field at the target	--	--	+
Symmetric configuration	-	++	+
Open mechanical structure	(+)	-	+
Large $\int B \cdot dl$ at small angles	+	--	+
High luminosity capability	-	+	+

Table II: Design considerations for the toroidal magnet

1) Size

time-of-flight path required for particle identification via momentum and β

$$L \geq 2 \text{ m for particles going sideways}$$

$$L \geq 3 \text{ m for particles going forward}$$

$$+ \text{ diameter} \approx 4 \text{ m, total length} \approx 4 \text{ m}$$

2) Field level

a) small destabilizing forces

b) momentum resolution $\Delta p/p \approx 1\%$

$$+ \int B \cdot dl \approx .5 \text{ T}\cdot\text{m} \quad + \text{ Amp}\cdot\text{turns} \approx 5 \cdot 10^6$$

3) Number of coils

- a) 4-fold symmetry for polarized target experiments
 - + 4, 8, 12, ...
- b) low obstruction of the ϕ -range due to the coils
 - + 8 coils

4) Coil shape

- a) no transverse focusing/defocusing effects due to r- and z-components of the field
 - + circular inner coil shape
- b) large $\int B \cdot dl$ in the forward direction
 - + asymmetric coil shape with longer forward part